J. Fluid Mech. (1968), *vol.* 31, *part* 4, *pp.* 669–688
Printed in Great Britain

The slow motion of a flat plate in a viscous stratified fluid

By SEELYE MARTIN† AND ROBERT R. LONG
Department of Mechanics, The Johns Hopkins University, Baltimore, Maryland

(Received 7 September 1967)

The existence of a 'wake' upstream of an obstacle moving slowly through a stratified fluid has been known for some time. The present study shows that a thin, flat plate moving slowly and horizontally through a linearly stratified salt-water mixture has, in addition, a boundary layer over the plate whose thickness increases upstream from the *back* of the plate.

The theory assumes that the ratio of diffusivity to viscosity is small, and that the plate moves so slowly that inertia forces are negligible; under these conditions, a similarity solution is derived describing the boundary layer over the plate. The study also shows that salt diffusion is important in a second, thinner boundary layer whose thickness increases from the front of the plate.

In the experiment, a plate was towed through a tank of linearly stratified salt water. From streak photographs of the boundary layer over the plate, it was possible to confirm quantitatively the similarity solution and to infer at very slow velocities the presence of the thin diffusion boundary layer.

1. Introduction

Experimental studies (Long 1955; Yih 1959) show that an obstacle moving slowly through a continuously stratified fluid creates an internal disturbance which propagates far upstream. This phenomenon is called blocking.

Blocking, and the analogous Taylor columns in rotating fluids, is the subject of much current research and controversy. It seems likely that it does not occur when the stratification is sufficiently slight or the motion of the obstacle sufficiently large (Long 1955). Such supercritical flow resembles potential flow, and all disturbances vanish at moderate distances upstream and downstream. When the flow becomes slow enough to permit waves to remain at rest with respect to the barrier, experiment and theory indicate that waves appear in the lee (figure 1, plate 1). In addition, experiment and theory (Long 1959; Trustrum 1964; Bretherton 1967) indicate that disturbances may also propagate upstream in the subcritical case; it is not known, however, whether these upstream disturbances are present when the obstacle is very small. The time-dependent analysis by Trustrum indicates that such upstream disturbances always occur in the subcritical case, but the approximations and simplifications of her analysis make her conclusion controversial. Very recently Drazin & Moore (1967) have

† Current address: Department of Meteorology, M.I.T., Cambridge, Massachusetts.

derived steady solutions, undisturbed upstream, over obstacles of special form and arbitrary size, but these solutions are certainly unstable when the barrier is large and will not be realized in experiment. Figure 2, plate 1, is an example of blocking in the form of jets over and upstream of the obstacle.

It seems obvious that viscosity strongly influences flows like that of figure 2. The main purpose of this investigation is to study blocking and the interrelated boundary layer over an obstacle at such very low velocities that viscous effects dominate the flow. Long (1959) initiated such studies by discovering a similarity solution describing the upstream wake of an obstacle moving through a linearly stratified viscous fluid of infinite extent. This solution is discussed briefly in §2. The present investigation, an extension of Long's (1959) paper, consists of a theoretical and experimental study of the steady motion of a finite flat plate through a viscous, stratified fluid. When the plate is moved slowly, a similarity solution exists describing a boundary layer over the plate, whose thickness increases upstream from the *back* of the plate. Section 2 contains the derivation of the differential equation describing the boundary layer. The same differential equation describes Long's upstream wake.

The experimental investigation consisted of towing a flat plate through the centre of a tank of linearly stratified salt water. Section 3 describes the apparatus in detail. Streak photographs, taken from a fixed camera, recorded the velocity field. Figure 3, plate 2, shows how to interpret the streak photographs. In the frame of the camera, alternate regions of upstream and downstream flow, and associated stagnation surfaces, characterize the velocity field over the plate. In all photographs of the velocity field, the plate is moving at a uniform velocity from left to right past a fixed camera.

Figure 4, plate 3, shows streak photographs of the boundary layer over the plate. The thickness of the region of backflow, which the two stagnation surfaces outline, decreases toward the back of the plate as the one-fourth power of the distance from the back. The similarity solution quantitatively describes the boundary layer shown in figure 3.

Section 4 compares the theoretical velocity profile with the experimental data, and discusses the effect on the boundary layer of salt diffusion at low velocities and inertia forces at high velocities. Section 4 also discusses the observations of the upstream and downstream wakes.

2. Theory

The following equations describe the steady, two-dimensional motion of a stratified fluid:

$$u\frac{\partial u}{\partial x}+v\frac{\partial u}{\partial y}=-\frac{\partial P}{\partial x}+\nu\nabla^2 u, \tag{1}$$

$$u\frac{\partial v}{\partial x}+v\frac{\partial v}{\partial y}=-\frac{\partial P}{\partial y}-\frac{\rho'}{\rho_0}g+\nu\nabla^2 v, \tag{2}$$

$$u\frac{\partial s}{\partial x}+v\frac{\partial s}{\partial y}=D\nabla^2 s, \tag{3}$$

$$u=-\frac{\partial \psi}{\partial y}, \quad v=\frac{\partial \psi}{\partial x}, \tag{4}$$

where x is the horizontal co-ordinate, y is the vertical co-ordinate, and u and v are the corresponding velocity components. The following expression relates the quantity P to the pressure p:

$$P = \frac{p}{\rho_0} + gy + \frac{g}{\rho_0}\int \bar{\rho}(y)\,dy. \tag{5}$$

The density ρ is written as $$\rho = \rho_0 + \bar{\rho}(y) + \rho', \tag{6}$$

where ρ_0 is the mean density, $\rho_0 + \bar{\rho}(y)$ is the undisturbed density distribution, and ρ' is the perturbation density.

In equations (1)–(4), we have made the Boussinesq approximation (Spiegel & Veronis 1960). This is accurate for salt-water solutions provided the density variations in the fluid are small. In the experiment, the density of the salt (NaCl) solution varied by 1·25% over the depth of the plate from the free surface. It can be shown from the empirical Jones–Dole formula (Stokes & Mills 1965) that the viscosity coefficient ν varies by 2% over this density variation, so that ν is constant to the order of the accuracy of the Boussinesq approximation.

On the other hand, the diffusion coefficient D varies by 8% as the density varies by 1·25% (see Harned 1959) so that D is *not* a constant within the accuracy of the Boussinesq approximation. In this section, however, D will be neglected from an order-of-magnitude argument, which is not affected by an error of 8%. In the appendix and §4, where D explicitly appears in the analysis, we show for the experiment that diffusion only acts on the velocity field in a salt boundary layer of maximum thickness 0·3 cm. Over this height, assuming salinity varies linearly with height, D varies by 0·2% (Harned 1959), so that for our purposes, we can assume D constant.

To the order of the accuracy of the Boussinesq approximation, we may write the empirical dependence of density on salinity (Harned & Owen 1958) as

$$\rho = \rho_0[1 + \epsilon(s - s_0)], \tag{7}$$

where s_0 is the mean salinity. The salinity s is measured in grams of solute per cubic centimetre of solution, and for NaCl in water, $\epsilon = 0{\cdot}7203$.

If we cross-differentiate equations (1) and (2), and substitute (4) and (7) into the resultant equation, then we obtain the following vorticity equation:

$$\left[\frac{\partial\psi}{\partial x}\frac{\partial}{\partial y} - \frac{\partial\psi}{\partial y}\frac{\partial}{\partial x} - \nu\nabla^2\right]\nabla^2\psi = -g\epsilon\frac{\partial s}{\partial x}. \tag{8}$$

For our problem, equations (3) and (8) describe the viscous diffusive motion of a stratified fluid.

If we assume that the undisturbed fluid is linearly stratified and in uniform motion, then the following boundary conditions describe flow over a finite flat plate (figure 5):

$$\left.\begin{aligned} &\text{at } y = 0, \quad 0 \leqslant x \leqslant L \quad \psi = 0, \frac{\partial\psi}{\partial y} = 0, \\ &\qquad\qquad\qquad\qquad\quad \frac{\partial s}{\partial y} = 0; \\ &\text{as } y \to \infty, \qquad\qquad\quad \psi = U_0 y, \quad \frac{\partial^2\psi}{\partial y^2} = 0, \\ &\qquad\qquad\qquad\qquad\quad s = -\frac{k}{\epsilon}y. \end{aligned}\right\} \tag{9}$$

(We choose $s = -(k/\epsilon)y$ so that $(1/\rho_0)|\partial\rho/\partial y| = k$.) Upstream and downstream of the plate, we have the integral requirement that the momentum flux

$$J = \int_{-\infty}^{+\infty} [P + u^2]\, dy \tag{10}$$

is constant (independent of x).

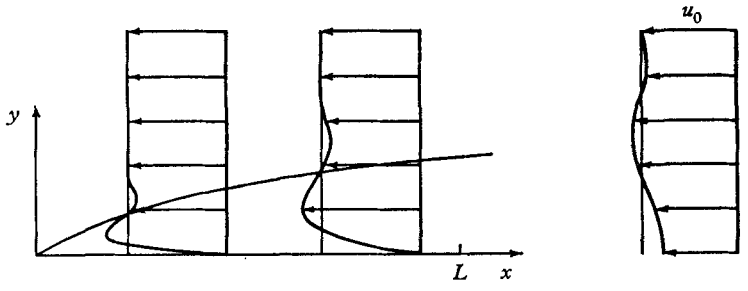

FIGURE 5. Co-ordinate system for flow over a finite plate.

Since equations (2) and (8) with the boundary conditions (9) and (10) are hardly tractable in their present form, we look for possible simplifications. In figures 3 and 4, plates 2 and 3, we see that the horizontal variations of velocity are much smaller than the vertical variations, so that we make the familiar boundary-layer approximation. If we also assume that the motion is so slow that inertia is unimportant,† then (8) and (3) become

$$g\epsilon \frac{\partial s}{\partial x} = +\nu \frac{\partial^4 \psi}{\partial y^4}, \tag{11}$$

$$\frac{\partial(\psi, s)}{\partial(x, y)} = D \frac{\partial^2 s}{\partial y^2}. \tag{12}$$

These equations are analogous to the equations describing the slow, viscous motion of an obstacle down the axis of a rotating fluid (for example see Herbert 1965).

Yih (1959), by neglecting the right-hand sides of equations (11) and (12), derived the stratified analogy to the Taylor–Proudman theorem. Also, Long (1962) derived the stratified analogy to the wakes found by Herbert (1965).

An important difference between salt-stratified solutions and rotating fluids is that the ratio of diffusivity to viscosity for salt water is

$$\frac{D}{\nu} \sim 10^{-3}.$$

The small size of this ratio means that we can neglect diffusion in (12), while retaining viscosity in (11). This approximation has *no* analogy in the previously mentioned rotating system, since the diffusion coefficient for angular momentum is simply ν.

† Janowitz (1967) has investigated the far flow field of an obstacle moving in a stratified fluid. In his analysis, he approximates the inertia terms by making the Oseen linearization.

The neglect of diffusion in (12) gives

$$\frac{\partial(\psi,s)}{\partial(x,y)} = 0, \quad \text{so that} \quad s = s(\psi). \tag{13}$$

Far from the plate, the boundary conditions (9) give

$$\psi = U_0 y \quad \text{and} \quad s = -(k/\epsilon)y,$$

so that the functional dependence of s on ψ becomes (Long 1959)

$$s = -\frac{k}{\epsilon U_0}\psi. \tag{14}$$

Equation (14) implies that any function satisfying the boundary conditions (9) on ψ also satisfies the boundary conditions on s. The appendix and §4 show (14) to be a very good approximation, except in the immediate vicinity of the plate where salt diffusion is important.

Substitution of (14) into equation (11) gives

$$\frac{\partial^4\psi}{\partial y^4} + \beta\frac{\partial\psi}{\partial x} = 0, \tag{15}$$

where $\beta = gk/U_0\nu$.

Equation (15) is parabolic (Courant & Hilbert 1962, vol. 2, p. 177), with the time-like variable x increasing upstream. Non-trivial solutions, then, only exist for x positive, so that (15) has no solutions describing a downstream wake.

Although (15) has no analogy in the equations describing the motion of obstacles along the axis of a rotating fluid, an identical equation describes slow, viscous flow in the meteorological beta-plane (for example see Long 1962). The results of this section, then, can be applied to the beta-plane.

We now discuss two particular similarity solutions of (15); one describing an upstream wake, the other describing the boundary layer over a flat plate.

The upstream wake

When we neglect inertia, the boundary condition (10) on the upstream wake becomes

$$J = \int_{-\infty}^{+\infty} P\,dy \tag{16}$$

for $x > L$. If we assume that far upstream of the plate, the wake is only determined by the magnitude of the momentum flux J, then equation (15) and condition (16) have the following similarity solution:

$$\psi = U_0 y + J(\beta/\nu x)^{\frac{1}{2}} g(\eta), \tag{17}$$

where

$$\eta = y\left(\frac{x}{\beta}\right)^{-\frac{1}{4}} = \frac{y}{(\nu U_0 x/kg)^{\frac{1}{4}}}.$$

Long (1959) describes the method of solving for $g(\eta)$. Figure 6, in which $g'(\eta)$ has been arbitrarily set equal to 1 at $\eta = 0$, shows the resultant horizontal velocity profile.

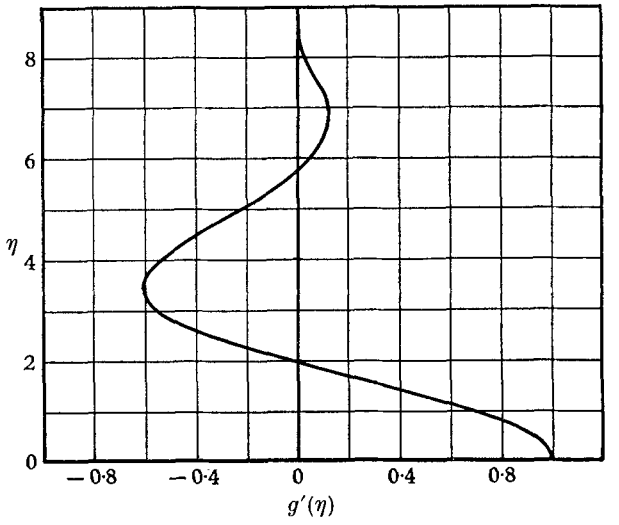

FIGURE 6. The horizontal velocity of the upstream wake solution.

The boundary-layer solution

We next discuss a similarity solution of (15) describing the flow over the plate. For a semi-infinite plate ($0 \leqslant x \leqslant \infty$), the solution of (15) takes the form

$$\psi = U_0(x/\beta)^{\frac{1}{4}} f(\eta), \tag{18}$$

where

$$\eta = \frac{y}{(U_0 \nu x/kg)^{\frac{1}{4}}}.$$

This solution can be applied to a finite plate by the following argument.† Because the time-like variable in (15) increases upstream, the flow over any finite section of the semi-infinite plate is unaffected by the flow upstream of the section. Therefore, we may truncate the semi-infinite plate to a plate of length L without altering the flow over the distance $0 \leqslant x \leqslant L$. The solution (18), then, for $(0 \leqslant x \leqslant L)$, describes the flow over both the finite plate and the semi-infinite plate.

Substitution of (18) into (15) gives the following ordinary differential equation:

$$4f^{\mathrm{iv}} - \eta f' + f = 0. \tag{19}$$

The boundary conditions (9) become

$$\left.\begin{aligned} &\text{at} \quad \eta = 0; \quad f = 0, \quad f' = 0; \\ &\text{as} \quad \eta \to \infty; \quad f = \eta, \quad f'' = 0. \end{aligned}\right\} \tag{20}$$

Equation (19) with the boundary conditions (20) is easily solved numerically. Figures 7 and 8 show graphs of the horizontal and vertical velocities.

For small η, the leading terms in the expansion of $f(2)$ were found numerically to be

$$f(\eta) = 1{\cdot}154\eta^2 - 0{\cdot}564\eta^3 + O(\eta^6) + \ldots. \tag{21}$$

† Van Dyke (1964) uses an analogous argument in his discussion of the Blasius solution.

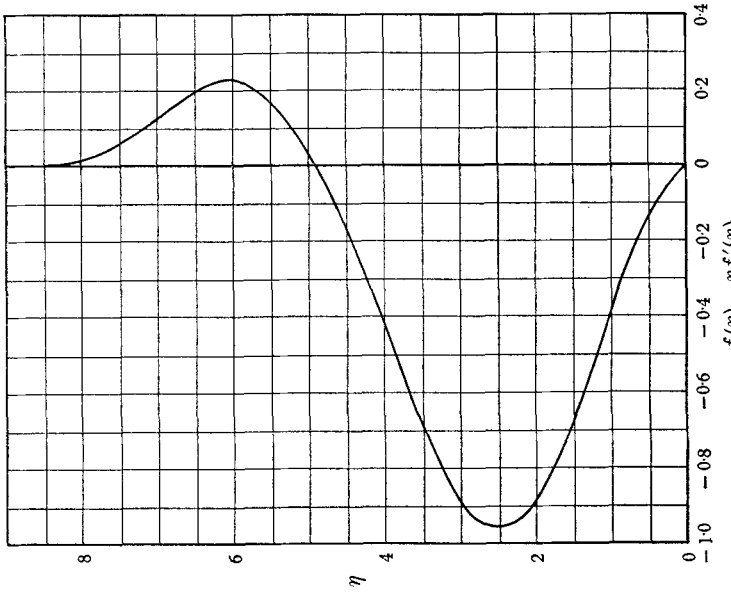

FIGURE 8. The vertical velocity of the boundary layer solution.

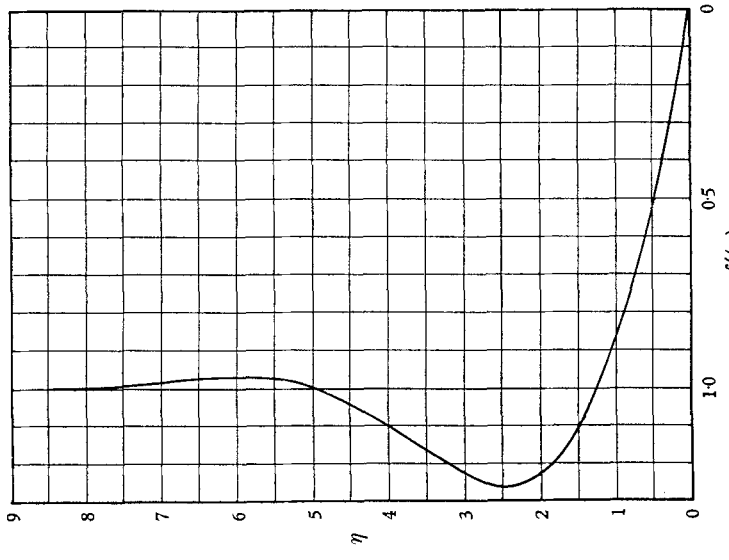

FIGURE 7. The horizontal velocity of the boundary layer solution.

For large η, the asymptotic solution to (19) was found to be

$$f(\eta) = \eta + B\exp\{-\tfrac{1}{2}a\eta^{\frac{4}{3}}\}\cos\left(\frac{\sqrt{3}}{2}a\eta^{\frac{4}{3}}\right)\left\{\frac{1}{\eta^{\frac{13}{3}}} + O\left(\frac{1}{\eta^{\frac{17}{3}}}\right)\right\}, \tag{22}$$

where $a = |3/4^{\frac{4}{3}}|$, and B is an undetermined constant. A typical term in the expansion of either u or v for large is

$$\exp\{-\tfrac{1}{2}a\eta^{\frac{4}{3}}\}\cos\left(\frac{\sqrt{3}}{2}a\eta^{\frac{4}{3}}\right),$$

so that as η goes to infinity, the velocity fluctuations fall to zero exponentially and oscillate with increasing frequency.

3. The Experiment

The apparatus

For the experimental study, we towed a flat plate through the middle of a long tank of linearly stratified salt water (figure 9, plate 3). The tank dimensions were 20 ft. long, 15 in. deep and 6·5 in. wide. A stainless steel track supported the flat plate at a height of 6 in. from the bottom of the tank. Three stainless steel pillars supported the track; two adjustable machine screws and a ball-bearing pivot set into the track served as a bearing surface between the track and the pillars. The pillars were mounted on a removable aluminum plate, so that we could dismantle and wash the entire apparatus after each experiment.

The track was 8 ft. long by 6 in. wide. Because of the three-point suspension, we could level the track to within $\frac{1}{32}$ of an inch. The material of the plate was $\frac{1}{16}$ in. hard brass; the plate dimensions were 3 ft. long by 5·5 in. wide. Teflon strips, fastened to the edges of the plate, served as bearing surfaces between the plate and the steel track. Since the coefficient of sliding friction for Teflon is the same as its coefficient of standing friction, the Teflon strips eliminated the problem of 'stick-slip' at slow velocities. To reduce glare in the streak photographs, the plate was painted flat black.

Piano wire connected the plate to a drum drive. The drum, 2 in. in diameter, was driven by a Bodine variable speed motor with a Minarek transmission. (For the Bodine–Minarek combination, the shaft speed is virtually independent of variations in the applied torque.) A pulley and counterweight system at the opposite end of the tank kept the wire taut.

We measured the velocity field of the fluid with streak photographs (figure 3, plate 2). The streak photographs were time exposures of a suspension of fine aluminium dust in the fluid, illuminated by an intense plane of light. Two cylindrical lenses collimated the output of a Sylvania Sun Gun II bulb into a plane. The resultant beam was about 0·8 cm thick and fanned from a width of 20 cm at the end of the lens system to 46 cm at the plate. A sheet of heat-absorbent glass, cooled by a blower, absorbed the infra-red radiation of the bulb. During the experiment, a black box covered the lens system, and the light field was centered over the plate.

A black screen placed behind the tank opposite the camera provided contrast in the photographs; a ruler placed in the light field provided scale. The camera,

a Graflex using 120 mm film, was tripod-mounted, and was levelled and aligned relative to the side of the tank.

There were a number of steps to filling the tank. To eliminate air bubbles, the water used in the experiment was allowed to settle for 48 h in two 55-gallon drums. One of the drums held a salt solution with a density of 1·022 g cm^{-3}, and the other held fresh water (ρ = 0·997 g cm^{-3}). We prepared solutions of densities by mixing the salt and fresh water in different proportions in a third container. The contents of the container were then introduced into the tank at the bottom. The first solution to flow into the tank was fresh water; the density of each successive layer was increased by a tenth of the maximum desired density. Eleven layers of water of different densities, but equal volumes, filled the tank to a depth of 12 in. Filling the tank took about 8 h.

To obtain a linear density gradient, we gently stirred the layered fluid at 4 ft. intervals along the length of the tank. The induced turbulent mixing smoothed the steps in the profile. Twelve to 15 h after stirring the fluid, the experiment began. During the course of an experiment, we measured the salinity profile with a Wheatstone bridge and a conductivity cell. Figure 10 displays a typical salinity profile measured at two different times in the course of an experiment.

The experiment began with the insertion of the plate into the fluid and connexion of the plate to the tow wire. Next, we injected a suspension of aluminum particles in water into the light field with a hypodermic syringe. As soon as the associated disturbances disappeared, the drive motor was started.

The point on the rail where the photographs were taken was 100 cm from the initial position of the front of the plate. To give the streak photographs of the velocity field the same scale for different plate velocities, we set the time exposure of the camera by the time for the plate to travel between 2·5 and 3 cm. The plate velocity and the time exposure were measured with a stop-watch. A typical experiment lasted for 9 h and consisted of five different runs. At the beginning of the separate runs, we injected aluminum particles into the fluid. At the end of an experiment, the entire apparatus was drained, dismantled, cleaned, and dried.

The data analysis

In the analysis, the photographs of the velocity field were enlarged two times actual size. On the photographs, a strong region of back flow characterized the velocity field over the plate (figure 3, plate 2). The heights above the plate of the two stagnation surfaces separating the region of back flow from the regions of upstream flow correspond to heights in a co-ordinate frame moving with the plate where the fluid velocity is equal to the free stream velocity. Rather than measure the complete velocity profile, we recorded only the heights of the two stagnation surfaces. These heights were then non-dimensionalized and compared with the theory.

We measured the heights of the first and second stagnation surfaces at 5 cm intervals along the plate. Since the plate moves past the fixed camera, we defined the average distance $\bar{x}$ of a reference point on a photograph as the average of the distances x of the points of the co-ordinate system of the plate, which pass the

reference point on the photograph during the time exposure. The maximum absolute error introduced by assuming that $x = \bar{x}$ was $\pm 1{\cdot}5$ cm. From the definition of η (18), the non-dimensional heights of the first and second stagnation surfaces are

$$\eta_{1s} = \frac{y_{1s}}{(\bar{x}U_0\nu/kg)^{\frac{1}{4}}} \quad \text{and} \quad \eta_{2s} = \frac{y_{2s}}{(\bar{x}U_0\nu/kg)^{\frac{1}{4}}}, \tag{23}$$

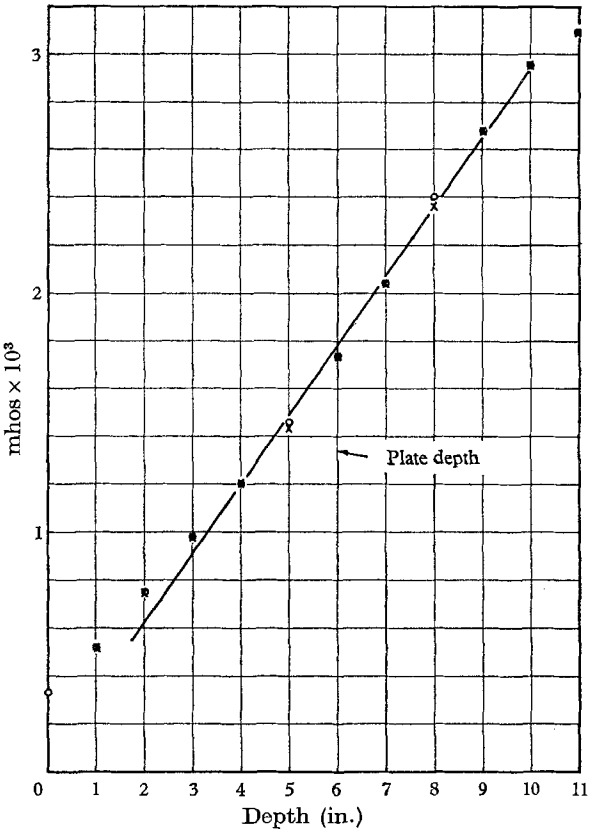

FIGURE 10. Graph of conductivity versus depth for a typical experiment. $T = 23$ °C. In the experiment, salinity is linearly proportional to conductivity to within 0·3 %. ○, 12·00 p.m.; ×, 4·00 p.m.

where the subscripts $1s$ and $2s$ refer to the first and second stagnation surfaces. The theoretical values of η_{1s} and η_{2s} are (from figure 7)

$$\eta_{1s} = 1{\cdot}25 \quad \text{and} \quad \eta_{2s} = 5{\cdot}00. \tag{24}$$

The percentage error of the experimental values of η_{1s} and η_{2s} in (23) is easily calculated. The error contribution from the assumption that $\bar{x}^{\frac{1}{4}} = x^{\frac{1}{4}}$ varied from 7 % at $\bar{x} = 5$ cm, to 0·5 % at $\bar{x} = 80$ cm. For $\bar{x} \geqslant 20$ cm, the error is less than 2 %.

The reading error of y_{1s} on the photographs is $\pm 0{\cdot}025$ cm, and of y_{2s}, $\pm 0{\cdot}05$ cm. In the experiment, y_{1s} varied between 0·2 and 0·6 cm, so that the percentage reading error of y_{1s} varied from 6 to 4 %. y_{2s} varied between 1 and 3 cm, so that its reading error varied from 5 to 2 %.

The value of the viscosity ν used in the calculation of η was the value of the viscosity at the level of the plate $\bar{\nu}$. We calculated $\bar{\nu}$ from the Jones–Dole formula (Stokes & Mills 1965), which gave

$$\bar{\nu}(T = 23\,^{\circ}\mathrm{C}, \rho = 1{\cdot}010\ \mathrm{g\ cm^{-3}}) = 9{\cdot}58 \times 10^{-3}\ \mathrm{cm^2\ sec^{-1}}.$$

(The water temperature during the runs varied between 23·0 and 23·4 °C.)

The viscosity ν varied by 2 % as the salinity varied from zero at the free surface to its value at the depth (15 cm) of the plate; over the depth of the boundary layer, ν varied by approximately 0·4 %. Thus $\bar{\nu}^{\frac{1}{4}}$ contributed an error of 0·1 % to η.

We calculated the density gradient k used in (23) by fitting a straight line to a plot of conductivity versus depth (figure 10). The accuracy of the fit was about 5 %, so that $k^{\frac{1}{4}}$ contributed an error of 1 % to η.

The percentage reading error of the velocity U_0 was less than 0·1 %.

Summation of all contributions to the reading error of (23) determined the accuracy of η_{1s} and η_{2s}. The minimum reading error was 6 and 4 %, respectively.

4. Comparison of theory with experiment

The boundary layer

Before comparing the measured values of η_{1s} and η_{2s} with the theory, let us first establish the range of validity of the similarity solution. Substitution of the similarity solution into the equations of motion shows that the ratio of the largest neglected term (the inertia term) to the retained viscous term is

$$\left(\frac{U_0^3}{\nu k g x}\right)^{\frac{1}{2}}. \tag{25}$$

It is therefore convenient to define an inertia length scale x_i such that

$$\frac{U_0^{\frac{3}{2}}}{(\nu k g)^{\frac{1}{2}} x_i^{\frac{1}{2}}} = \tfrac{1}{10}. \tag{26}$$

Inertia forces should be negligible† and the similarity solution should describe the flow for

$$x > x_i, \tag{27}$$

or away from the back of the plate.

Derivation of an analogous diffusion length scale is more complicated; the details are given in the appendix. We see there that salt diffusion acts in a boundary layer growing from the front of the plate. Since the thickness of the non-diffusive boundary layer increases from the back of the plate, there will be a point over the plate where the salt boundary layer thickness is non-negligible compared with the non-diffusive thickness. At slow enough velocities, then, the effects of salt diffusion should be visible in the experiment near the back of the plate. We find that we may define a diffusion length x_{dl} by the equation

$$\frac{1}{10}\left(\frac{x_{dl}}{L}\right)^{\frac{1}{4}} = \left(1 - \frac{x_{dl}}{L}\right)^{\frac{1}{3}} \left(\frac{D^2 U_0^3}{A^2 \nu^3 L g k}\right)^{\frac{1}{6}}, \tag{28}$$

† Other neglected terms are still smaller provided $U_0 x_i/\nu > 1$. This condition is satisfied for the experiments.

where L is the length of the plate and $A = 1{\cdot}154$. We may neglect diffusion in our problem provided

$$x > x_{dl}. \tag{29}$$

From (27) and (29), both inertia and diffusion are important near the back of the plate. Of course, the length scales are only order-of-magnitude estimates of the distances over which diffusion and inertia affect the flow.

Using a plate of length $L = 91{\cdot}5$ cm, we performed five different experimental runs covering the range of validity of the similarity solution. Table 1 in the text summarizes the parameters of the five runs and lists $U_0 x_i/\nu$, x_i and x_{dl}. The table suggests that diffusion effects should be visible in the first two runs; inertia effects, in the last two.

U_0 (cm sec^{-1} $\times 10^{-2}$)	Water temp. (°C)	Density gradient (cm$^{-1} \times 10^{-4}$)	$\frac{U_0 x_i}{\nu}$	x_i (cm)	x_{dl} (cm)
2·85	23·0	8·33	0·9	0·3	70
5·24	23·4	8·33	10	1·9	4
8·41	23·4	8·61	67	7	10^{-1}
11·25	23·4	8·61	211	18	10^{-2}
14·5	23·4	8·61	575	38	10^{-4}

TABLE 1. Parameters of the experimental runs

Before describing the effects of diffusion and inertia in the experiment, let us point out for the five runs that the similarity solution only describes the experimental flow to a height of $\eta = 5$. Comparison of the theoretical vertical velocity profile (figure 8) with the experimental photographs shows that above the second stagnation surface ($\eta = 5$), the theoretical vertical velocity is positive, whereas the observed vertical velocity is negative. Also, the velocity oscillations predicted by the asymptotic solution (22) for large η do not appear; instead we observed above the second stagnation surface a wide region of upstream flow, whose height does not decrease toward the back of the plate. It can be shown from the asymptotic solution that the inertia terms cause the deviation from the similarity solution for large values of η. Since $\eta = 5$ is the height of the second stagnation surface, it is convenient experimentally to take the thickness of the non-diffusive boundary layer to be

$$\delta(x) \simeq 5\left(\frac{U_0 \nu x}{kg}\right)^{\frac{1}{4}}. \tag{30}$$

We now discuss the quantitative behaviour of the experimental velocity field. Table 1 predicts that the best agreement between theory and experiment will occur for $8{\cdot}4 \times 10^{-2}$ cm sec^{-1}. Figure 11 shows that η_{1s} and η_{2s} in this case agree with theory to within 4% for 10 cm $\leqslant \bar{x} \leqslant$ 80 cm. In its region of validity, the similarity solution predicts the correct value of η_{1s} and η_{2s}.

At slower velocities, table 1 suggests that diffusion affects the velocity profile. For $5{\cdot}24 \times 10^{-2}$ cm sec^{-1} and $2{\cdot}85 \times 10^{-2}$ cm sec^{-1}, figure 11 shows that the values of η_{1s} and η_{2s} deviate from the predicted values near the back of the plate,

and that the largest deviations occur for the slowest velocities. At the slowest velocity, $2{\cdot}85 \times 10^{-2}$ cm sec^{-1}, evaluation at the back of the plate of the thickness δ_u (defined in the appendix) of the region of the velocity perturbation caused by diffusion gives

$$\delta_u = 0{\cdot}34 \text{ cm}.$$

For $2{\cdot}85 \times 10^{-2}$ cm sec^{-1}, figure 12 shows that the height of the first stagnation surface η_{1s} decreases with $\bar{x}$ from $\bar{x} = 80$ cm to $\bar{x} = 15$ cm, then *increases* to 0·4 cm, or of order δ_u, at $\bar{x} = 5$ cm. y_{1s} achieves its largest value at $\bar{x}\,5 =$ cm for the slowest velocity of the five runs. This behaviour of y_{1s} for the slowest velocity may be the direct result of the salt boundary layer growing downstream beneath the non-diffusive boundary layer.

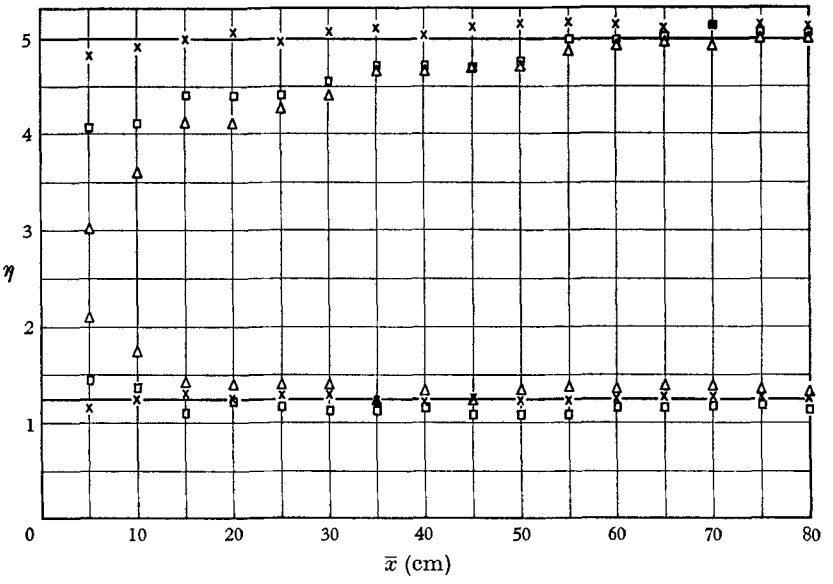

FIGURE 11. Non-dimensional heights of the stagnation surfaces versus distance from the back of the plate for the three slow runs. △, $2{\cdot}8 \times 10^{-2}$ cm sec^{-1}; □, $5{\cdot}2 \times 10^{-2}$ cm sec^{-1}; ×, $8{\cdot}4 \times 10^{-2}$ cm sec^{-1}.

In summary, our analysis predicts when salt diffusion will affect the non-diffusive boundary layer, but not how. Hopefully, by carrying our analysis much farther, we will be able to explain quantitatively the interaction between the non-diffusive boundary layer and the salt boundary layer.

Let us now discuss the effect of inertia on the solution. For the two higher velocities, table 1 shows that the effect of diffusion is negligible and that inertia is important near the back of the plate. Figure 13, which displays η_{1s} and η_{2s} for the two higher velocities, shows that except for $1{\cdot}125 \times 10^{-1}$ cm sec^{-1} and $\bar{x} \geqslant 70$ cm, the experimental values of η_{1s} fall below the predicted value of $\eta_{1s} = 1{\cdot}25$ by 12 to 25%, or well outside of the allowed reading error. The inertia length scale, then, which for $1{\cdot}125 \times 10^{-1}$ cm sec^{-1} predicts agreement for $\bar{x} \geqslant$ 18 cm, gives only an order-of-magnitude estimate of the distance over which inertia affects the flow.

The wakes

A quantitative attempt to verify the similarity solution describing the upstream wake failed. The observed flow (figure 4*a* and 14, plates 3 and 4) has a qualitative resemblance to the theoretical profile. Because the solution is independent of

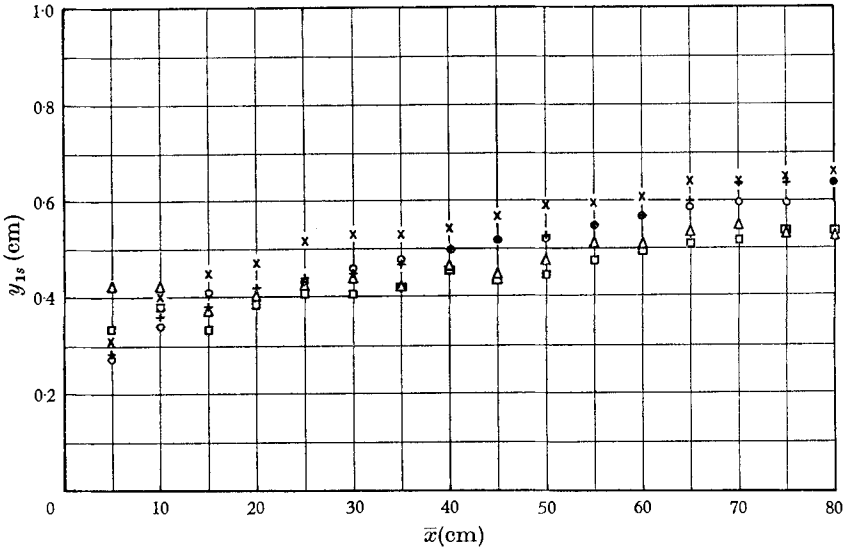

FIGURE 12. Height of the first stagnation surface versus distance from the back of the plate. +, $1{\cdot}45\times10^{-1}$ cm sec^{-1}; ○, $1{\cdot}12\times10^{-1}$ cm sec^{-1}; ×, $8{\cdot}41\times10^{-2}$ cm sec^{-1}; □, $5{\cdot}24\times10^{-2}$ cm sec^{-1}; △, $2{\cdot}85\times10^{-2}$ cm sec^{-1}.

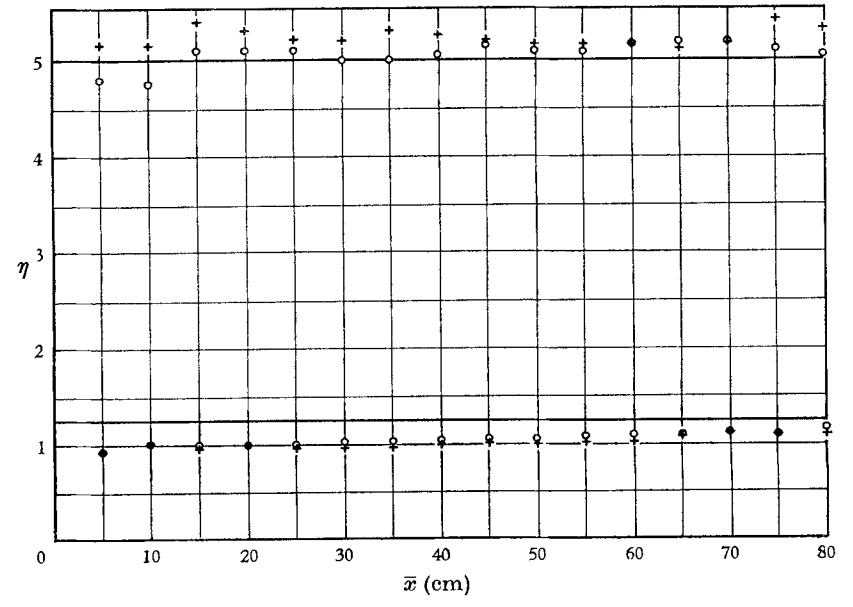

FIGURE 13. Non-dimensional heights of the stagnation surfaces versus distance from the back of the plate for the two faster runs. ○, $1{\cdot}125\times10^{-1}$ cm sec^{-1}; +, $1{\cdot}450\times10^{-1}$ cm sec^{-1}.

the shape of the obstacle which creates the disturbance, we only accept the solution to describe the flow far upstream of the plate. The short track, however, did not seem to provide enough travel time for the wake to become fully developed as the shear layers weakened and died out 30 to 50 cm upstream of a plate of 15 cm length, after the plate had travelled 100 cm. A longer track might well lead to a quantitative confirmation of the similarity solution describing the upstream wake.†

For the range of velocities over which the similarity solution describes the non-diffusive boundary layer and the observed upstream wake has an oscillatory profile in the vertical, the observed downstream wake has a simple velocity defect (figure 4*b*, plate 3). If we are far enough downstream of the plate so that we are in the region of the diffusive wake discussed by Long (1962), then the downstream wake should develop oscillations in the vertical; however, a 3 min time exposure taken 40 cm downstream of a 15 cm plate moving at $2{\cdot}85 \times 10^{-2}$ cm $\sec^{-1}$ and for $k = 8{\cdot}6 \times 10^{-4}$ cm^{-1} still showed a simple velocity defect. Oscillatory wake profiles have been observed both upstream and downstream of an obstacle moving down the axis of a rotating fluid (T. Maxworthy 1966, personal communication); this case is mathematically analogous to Long's diffusive solution (see Childress 1964; or Herbert 1965). Janowitz (1967) has found solutions for the non-diffusive downstream wake, but at the present time, these have not been confirmed by experiment.

The effects of higher velocities

The boundary-layer thickness continues to increase from the back of the plate at higher velocities. Figure 15, plate 5, shows the back of the plate 91·5 cm long,

$$U_0 = 4{\cdot}0 \times 10^{-1} \text{ cm sec}^{-1}, \quad k = 8{\cdot}61 \times 10^{-4} \text{ cm}^{-1} \quad \text{and} \quad x_i = 810 \text{ cm}.$$

Although the similarity solution does not describe the boundary-layer profile, the boundary-layer thickness still increases from the back of the plate. Above the second stagnation surface, shear layers growing from the back of the plate, characterize the flow. The dying-out of the shear layers upstream indicates that the flow is time-dependent, so that we made no quantitative measurements at higher velocities.

Since the entire depth of fluid above the plate is excited, a relevant parameter for describing the motion of the fluid in figure 15 is the internal Froude number F based on the depth of the plate from the free surface ($H = 15{\cdot}4$ cm). For $U_0 = 4{\cdot}0 \times 10^{-1}$ cm $\sec^{-1}$; $F = U_0/(kgH^2)^{\frac{1}{2}} = 2{\cdot}84 \times 10^{-2}$. Downstream of the long plate at this Froude number, we observed internal waves, which are not shown because of the low quality of the photographs. Qualitatively, however, they resembled those shown in figure 16, plate 6), which is a composite photograph of the flow of a plate 0·63 cm long moving at approximately the same Froude number, or $F = 2{\cdot}88 \times 10^{-2}$.

The plate in figure 16 has moved a distance of 2·8 cm past the camera during the time exposure, so that the swirls downstream of the plate would look like

† Y. H. Pao (1966, private communication) claims to have verified the upstream wake experimentally.

waves in a co-ordinate system attached to the plate. The qualitative resemblance between figures 15 and 16 is evidence that F is important in determining the flow at higher velocities.

The flows in figures 15 and 16 have the following properties: the shear layers above and ahead of the plate alternate in direction and grow from the back of the plate; the magnitude of the velocity fluctuations away from the plate is much less than the plate velocity; and in figure 16, the magnitude of the upstream jets is of the same order as the magnitude of the downstream waves.

We finally attempted to determine the velocity at which the boundary layer begins to grow downstream. The fastest experiment was for $U_0 = 1{\cdot}9$ cm sec^{-1}, $L = 91{\cdot}5$ cm, $k = 2{\cdot}67 \times 10^{-3}$ cm^{-1}; or $F = 7{\cdot}7 \times 10^{-2}$. The boundary-layer thickness still increased from the back of the plate. We were not able to move the plate fast enough to observe a boundary layer which grew downstream.

The authors wish to acknowledge the help of Mr Edward Bertic, Mr Michael Karweit and Mr Frank Troska in the building and carrying out of the experiment. This investigation was supported by the Office of Navel Research under Task Order no. NR-082-104, Contract no. Nonr-4010(01) and by Environmental Science Service Administration under Grant no. E-9-67(G).

Appendix. The salt boundary layer

To derive the form of the salt boundary layer, we scale the dimensional variable used in §2 as follows:

$$y' = \gamma y, \quad \psi' = \frac{\gamma\psi}{U_0}, \quad x' = \frac{x}{L} \quad \text{and} \quad s' = \frac{\gamma}{k\epsilon}s, \tag{A1}$$

where

$$\gamma = \left(\frac{gk}{U_0\nu L}\right)^{\frac{1}{4}},$$

and the primes denote non-dimensional variables.

Substitution of (A1) into equations (11) and (12) and dropping the primes from the variables gives

$$\frac{\partial^4\psi}{\partial y^4} = \frac{\partial s}{\partial x}, \tag{A2}$$

$$\frac{\partial(\psi, s)}{\partial(x, y)} = \frac{\partial\psi}{\partial x}\frac{\partial s}{\partial y} - \frac{\partial\psi}{\partial y}\frac{\partial s}{\partial x} = \alpha\frac{\partial^2 s}{\partial y^2}, \tag{A3}$$

where

$$\alpha = \frac{D}{\nu}\left(\frac{U_0^3}{\nu g k L}\right)^{\frac{1}{2}}.$$

Evaluation of (A3) at $y = 0$ over the plate gives the following boundary condition:

$$\frac{\partial^2 s}{\partial y^2} = 0 \quad \text{at} \quad y = 0. \tag{A4}$$

On the other hand, evaluation of the non-diffusive salinity field (from equation (14)) at $y = 0$ gives

$$\left.\frac{\partial^2 s}{\partial y^2}\right|_{y=0} = -\left.\frac{\partial^2\psi}{\partial y^2}\right|_{y=0} = -x^{-\frac{1}{4}}f''(0) = -1{\cdot}154x^{-\frac{1}{4}}. \tag{A5}$$

The numerical constant in (A 5) comes from (20). Since x is of order 1 in (A 5), the second derivative of the non-diffusive salinity field is at least of order 1 at the plate, so that condition (A 4) cannot be satisfied by the non-diffusive salinity field. Retention of diffusion in the problem, then, creates a region of non-uniformity at the plate.

We may eliminate the region of non-uniformity through use of the following asymptotic expansions of s and ψ and by stretching y as follows:

$$\left.\begin{aligned} \psi &= \alpha^{\frac{2}{3}} A^{\frac{1}{3}} \psi_1 + \frac{\alpha^2}{A} \psi_2 + \ldots., \\ s &= \alpha^{\frac{2}{3}} A^{\frac{1}{3}} s + \frac{\alpha^2}{A} s_2 + \ldots., \\ y &= (\alpha/A)^{\frac{1}{3}} y_d, \end{aligned}\right\} \tag{A 6}$$

where $A = 1{\cdot}154$.

For future convenience, we also set $x = 1 - x_d$. We assume that all of the subscripted variables are of order 1 in the region where diffusion is important.

By applying the matching procedure described in Van Dyke (1964), we derive the following boundary conditions on ψ_1 and s_1:

at $y_d = \infty$,

$$\left.\begin{aligned} \psi_1(x_d, \infty) &= \frac{y_d^2}{A} \frac{\partial^2}{\partial y^2} [(1-x_d)^{\frac{1}{4}} f(\eta)]_{y=0} = +y_d^2 (1-x_d)^{-\frac{1}{4}}, \\ \frac{\partial^2 s_1}{\partial y_d^2} &= -(1-x_d)^{-\frac{1}{4}}, \end{aligned}\right\} \tag{A 7}$$

and at $y_d = 0$,

$$\frac{\partial \psi_1}{\partial y_d} = \frac{\partial \psi_1}{\partial x_d} = \frac{\partial^2 s_1}{\partial y_d^2} = 0.$$

In (A 7), we use the expansion of $f(\eta)$ for small η given by equation (21).

Substitution of (A 6) into equation (A 2) gives

$$\frac{\partial^4 \psi_1}{\partial y_d^4} = -\alpha^{\frac{4}{3}} A^{\frac{1}{3}} \left[\frac{\partial^4 \psi_2}{\partial y_d^4} + \frac{\partial s_1}{\partial x_d} \right]. \tag{A 8}$$

To order $\alpha^{\frac{4}{3}}$, $\partial^4 \psi_1 / \partial y_d^4 = 0$, so that a solution of (A 8) satisfying the boundary conditions on ψ_1 is

$$\psi_1 = y_d^2 (1-x_d)^{-\frac{1}{4}}. \tag{A 9}$$

Equation (A 9) is simply the first term in the expansion of the non-diffusive stream function for small η. To order $\alpha^{\frac{4}{3}}$, then, the stream function in the salt boundary layer is the non-diffusive stream function. In the experiment, the maximum value of α was 0·26, which corresponds to $\alpha^{\frac{4}{3}} = 0{\cdot}17$.

Substitution of (A 9) into the diffusion equation gives

$$\frac{\partial s_1}{\partial x_d} - \frac{1}{8} \frac{y_d}{(1-x_d)} \frac{\partial s_1}{\partial y_d} = \frac{(1-x_d)^{\frac{1}{4}}}{y_d} \frac{\partial^2 s_1}{\partial y_d^2}. \tag{A 10}$$

Gevrey (1913, chapter 2), shows that (A 10) is a parabolic equation with the time-like variable x_d increasing from the front of the plate, so that the salt boundary layer should grow from the front of the plate. Since the non-diffusive boundary layer grows from the back of the plate, our analysis is only correct away from

the back of the plate, or where the salt boundary-layer thickness is much less than the non-diffusive boundary-layer thickness.

We may find the form of the solution to equation (A 10) and the boundary conditions (A 7) in the following way. Expansion of $(1-x_d)^{\frac{1}{4}}$, $(1-x_d)^{-1}$ and $(1-x_d)^{-\frac{1}{4}}$ around $x_d = 0$ in (A 7) and (A 10) gives

$$\frac{\partial s_1}{\partial x_d} - \tfrac{1}{8}(1 + x_d + x_d^2 + \ldots)\frac{\partial s_1}{\partial y_d} = (1 - \tfrac{1}{4}x_d - \tfrac{3}{32}x_d^2 + \ldots)\, y_d^{-1}\frac{\partial^2 s_1}{\partial y_d^2}; \tag{A 11}$$

at $y_d = 0$, $$\frac{\partial^2 s_1}{\partial y_d^2} = 0,$$

and as $y_d \to \infty$, $$\frac{\partial^2 s_1}{\partial y_d^2} = -(1 + \tfrac{1}{4}x_d + \tfrac{5}{32}x_d^2 + \ldots). \tag{A 12}$$

Equations (A 11) and (A 12) have the following solution:

$$s_1(x_d, y_d) = x_d^{\frac{2}{3}} \sum_{n=0}^{\infty} x_d^n s_n(\zeta), \tag{A 13}$$

where $$\zeta = y_d / x_d^{\frac{1}{3}}.$$

Substitution of (A 13) into (A 11) and (A 10) gives to order x_d a two-point boundary value problem for $s_0(\zeta)$.

$$s_0''(\zeta) + \frac{\zeta^2}{3} s_0'(\zeta) - \tfrac{2}{3} s_0(\zeta) = 0; \tag{A 14}$$

at $\zeta = 0$, $$s_0''(\zeta) = 0,$$

and as $\zeta \to \infty$, $$s_0''(\zeta) = -1.$$

The derivation of equations which describe $s_1(\zeta)$, $s_2(\zeta)$,... is equally straightforward.

Without solving (A 14), we can now obtain an order-of-magnitude estimate of the velocities at which diffusion will affect the non-diffusive boundary layer. The form of the solution (A 13) suggests that the salt boundary-layer thickness increases from the front of the plate as $x_d^{\frac{1}{3}}$. In dimensional variables, then, the thickness $\delta_s(x)$ of the salinity perturbation created by diffusion increases as

$$\delta_s(x) \sim \frac{\alpha^{\frac{1}{3}}}{A^{\frac{1}{3}}\gamma}\left(1 - \frac{x}{L}\right)^{\frac{1}{3}} = \left(\frac{D^4 U_0^9 L}{A^4 \nu^3 (gk)^5}\right)^{\frac{1}{12}}\left(1 - \frac{x}{L}\right)^{\frac{1}{3}}. \tag{A 15}$$

As we show in § 4, the thickness of the non-diffusive boundary layer increases as

$$\delta(x) \simeq 5\left(\frac{U_0 \nu x}{gk}\right)^{\frac{1}{4}}. \tag{A 16}$$

If we assume that the scale factor 5 also appears in (A 15), then

$$\delta_s(x) = 5\left(\frac{D^4 U_0^9 L}{A^4 \nu^3 (gk)^5}\right)^{\frac{1}{12}}\left(1 - \frac{x}{L}\right)^{\frac{1}{3}}. \tag{A 17}$$

In the experiment, however, we measure the u-velocity field, not the salinity field. From the scaling (A 6), the magnitude of the diffusive contribution to the u-velocity field is of order

$$\frac{\partial \psi_2}{\partial y_d} \sim \alpha^{\frac{5}{3}},$$

or an order α smaller than the diffusive salinity field. Therefore, we assume that the thickness $\delta_u(x)$ of the u-velocity perturbation created by diffusion is an order α smaller than $\delta_s(x)$, so that

$$\delta_u(x) = \alpha \delta_s(x). \tag{A 18}$$

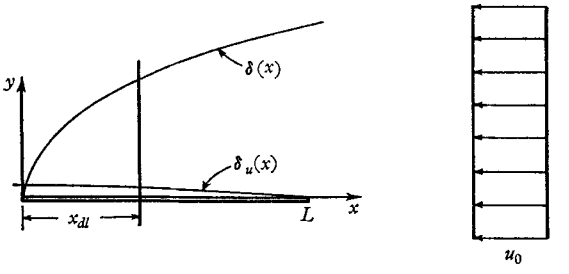

FIGURE 17. Sketch of $\delta_u(x)$ and $\delta(x)$ for the flow of a stratified diffusive fluid over a flat plate.

To derive a diffusion length scale, we assume that (A 17) and (A 18) give the correct order-of-magnitude of $\delta_u(x)$ over the entire length of the plate. We also assume that the effect of diffusion on the u-velocity profile will be visible in the experiment when

$$\delta_u(x) \geqslant \tfrac{1}{10}\delta(x) \quad \text{(figure 17)}.$$

We define the diffusion length scale x_{dl} as that distance for which

$$\delta_u(x_{dl}) = \tfrac{1}{10}\delta(x_{dl}),$$

or from (A 15) to (A 18),

$$\frac{1}{10}\left(\frac{x_{dl}}{L}\right)^{\frac{1}{4}} = \left(\frac{D^2 U_0^3}{A^2 L \nu^3 g k}\right)^{\frac{1}{6}} \left(1 - \frac{x_{dl}}{L}\right)^{\frac{1}{3}}. \tag{A 19}$$

The effects of diffusion should be negligible in the experiment for $x \geqslant x_{dl}$. (We calculated the value of D used in (A 19) from measurements of D at $T = 25\,^{\circ}\mathrm{C}$ (Stokes 1950). We extrapolated his result to $T = 23\,^{\circ}\mathrm{C}$ using the Nerst–Einstein equation (Jost 1960) and obtained

$$D(T = 23\,^{\circ}\mathrm{C}, \bar{\rho} = 1{\cdot}010 \text{ g cm}^{-3}) = 1{\cdot}40 \times 10^{-5} \text{ cm}^2 \text{ sec}^{-1}$$

as the mean diffusivity of our experimental solution.)

REFERENCES

BRETHERTON, F. P. 1967 The time-dependent motion due to a cylinder moving in an unbounded rotating or stratified fluid. *J. Fluid Mech.* **28**, 545.

CHILDRESS, S. 1964 The slow motion of a sphere through a viscous rotating fluid. *J. Fluid Mech.* **20**, 305–14.

COURANT, R. & HILBERT, D. 1962 *Methods of Mathematical Physics*, vol. II. New York: John Wiley.

DRAZIN, P. G. & MOORE, D. W. 1967 Steady two-dimensional flow of fluid of variable density over an obstacle. *J. Fluid Mech.* **28**, 353.

GEVREY, M. 1913 Sur les equations aux derivées partialles du type parabolic. *J. Math.* **9**, 305–475.

HARNED, H. S. 1959 Diffusion and activity coefficients of electrolytes in dilute aqueous solutions. *The Structure of Electrolytic Solutions* (ed. W. J. Hamer). New York: John Wiley.

HARNED, H. S. & OWEN, B. B. 1958 *The Physical Chemistry of Electrolytic Solutions*, 358–365. New York: Reinhold Publishing Corporation.

HERBERT, D. M. 1965 A laminar jet in a rotating fluid. *J. Fluid Mech.* **23**, 65–75.

JANOWITZ, G. 1967 On wakes in stratified fluids. *Tech. Rept.* no. 22 (*ONR series*). Department of Mechanics, The Johns Hopkins University.

JOST, W. 1960 *Diffusion*. New York: Academic Press.

LONG, R. R. 1955 Some aspects of the flow of stratified fluids. III. Continuous density gradients. *Tellus*, **7**, 342–57.

LONG, R. R. 1959 The motion of fluids with density stratification. *J. Geophys. Res.* **64**, 2151–63.

LONG, R. R. 1960 A laminar planetary jet. *J. Fluid Mech.* **7**, 632–8.

LONG, R. R. 1962 Velocity concentrations in stratified fluids. *J. Hydraulics Div. ASCE*, **88**, 9–26.

SPIEGEL, E. A. & VERONIS, G. 1960 On the Boussinesq approximation for a compressible fluid. *Astrophys. J.* **131**, 442–7.

STOKES, R. H. 1950 The diffusion coefficients of eight uni-univalent electrolytes in aqueous solution at 25 °C. *J. Am. Chem. Soc.* **72**, 2243–57.

STOKES, R. H. & MILLS, R. 1965 *Viscosity of Electrolytes and Related Properties*. Oxford: Pergamon Press.

TRUSTUM, K. 1964 Rotating and stratified fluid flow. *J. Fluid Mech.* **19**, 415–32.

VAN DYKE, M. 1964 *Perturbation Methods in Fluid Mechanics*. New York: Academic Press.

YIH, C. S. 1959 Effect of density variation on fluid flow. *J. Fluid Mech.* **8**, 481–508.

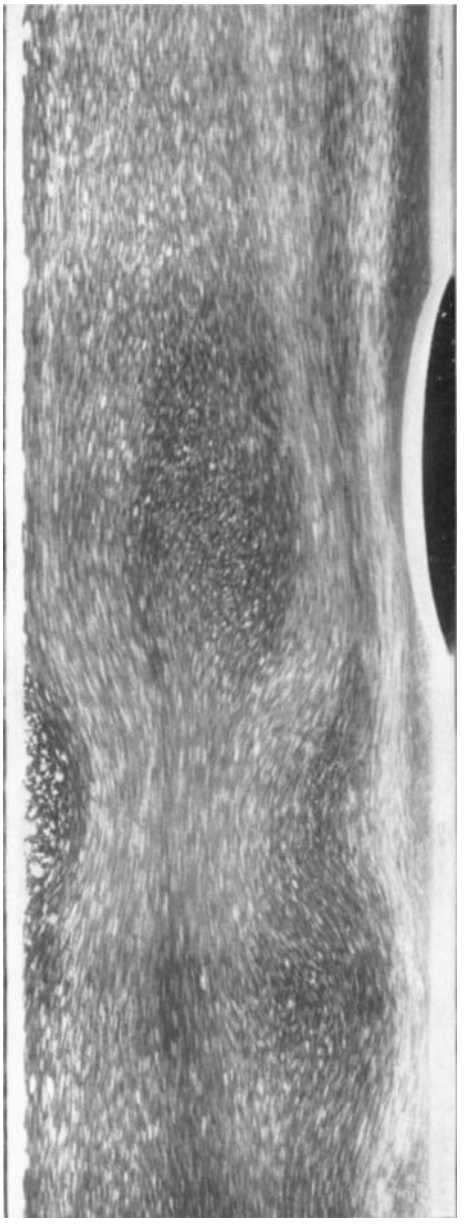

FIGURE 1. Flow of a stratified salt-water mixture over an obstacle. The stratification is nearly linear. The basic flow is from right to left.

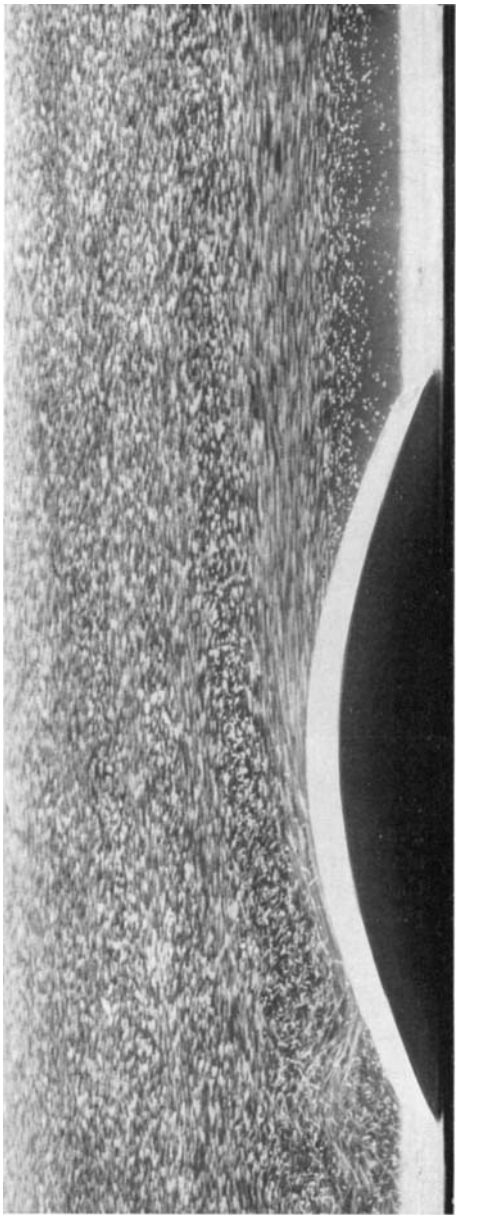

FIGURE 2. Multiple jets in the flow of a stratified fluid over a barrier.

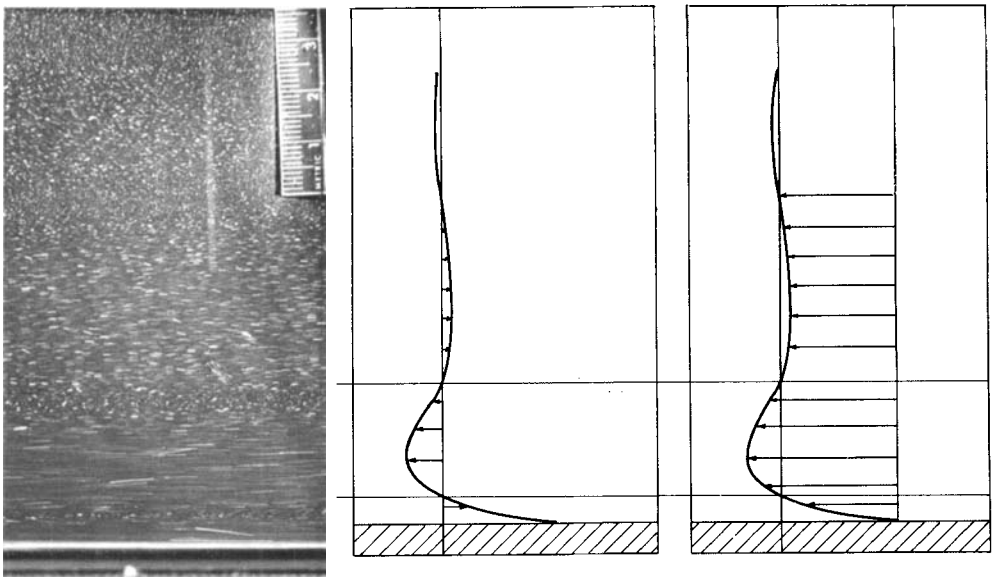

FIGURE 3 (*a*). Streak photograph of velocity field. Plate is moving from left to right past a stationary camera. (*b*) Sketch of velocity field of (*a*) in a co-ordinate system attached to the camera. (*c*) Sketch of velocity field of (*a*) in a co-ordinate system attached to the plate.

(*a*)

(*b*)

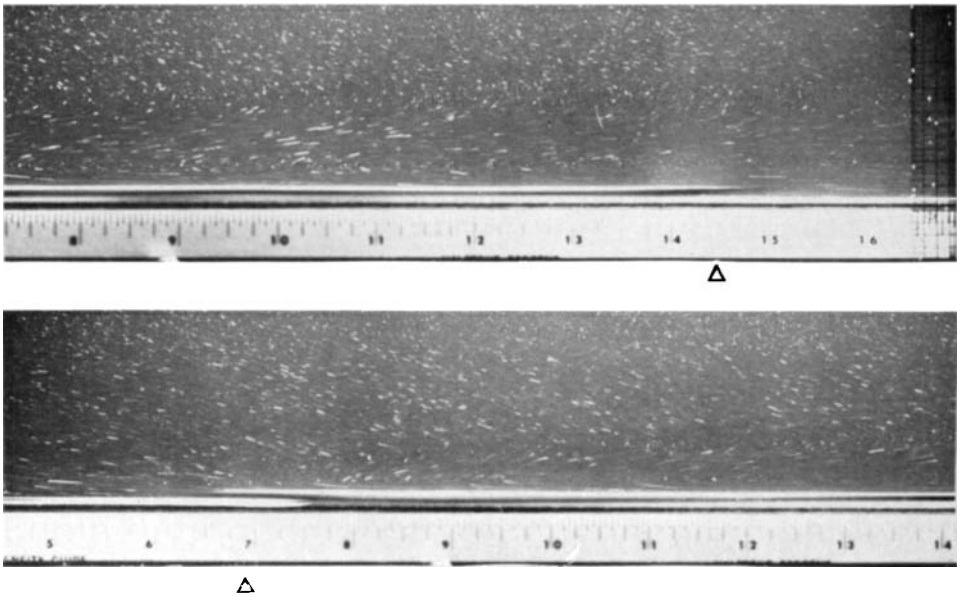

FIGURE 4. The boundary layer over the plate. Streak photographs of a plate 91·5 cm long, moving with a velocity of $7{\cdot}5 \times 10^{-2}$ cm sec^{-1} from left to right past a fixed camera. The constant density gradient is $(1/\rho_0)|\partial\rho/\partial y| = 8{\cdot}4 \times 10^{-4}$ cm^{-1} and the time exposure is 30 sec. The arrows mark the mean position of the front and the back of the plate. (*a*) Front of the plate. (*b*) Back of the plate.

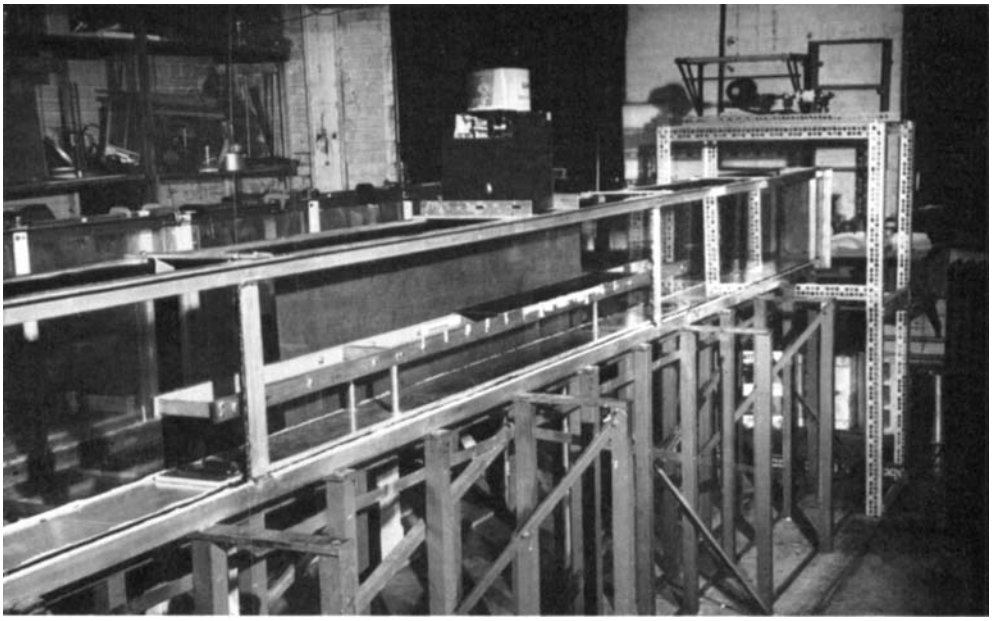

FIGURE 9. The apparatus.

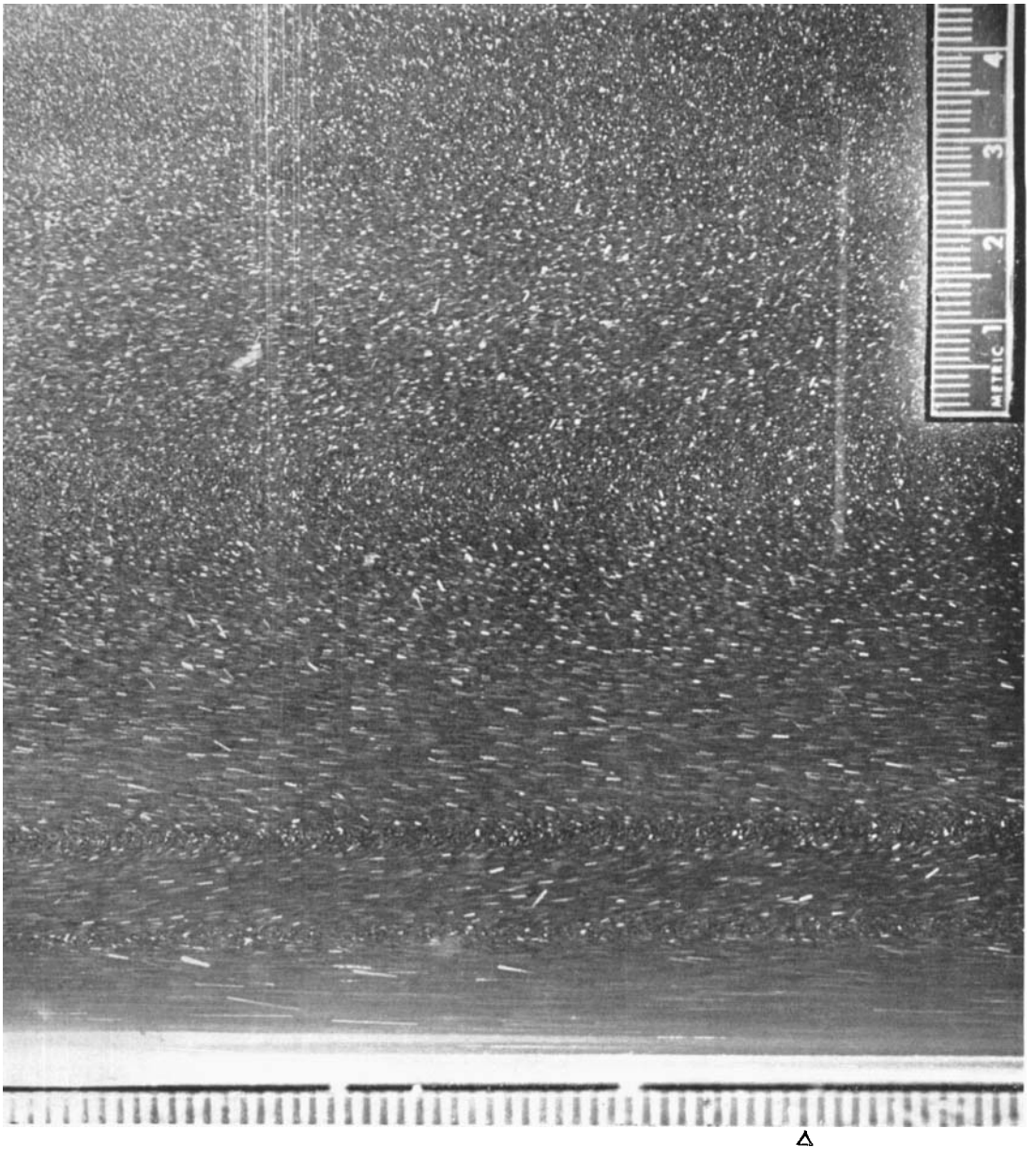

FIGURE 14. The upstream wake. Arrow is 25 cm upstream of the front of a plate 15 cm long. Camera is stationary; plate is moving from left to right. $U_0 = 1{\cdot}45\ 10^{-1}$ cm sec^{-1}; $k = 8{\cdot}6\ 10^{-4}$ cm^{-1}.

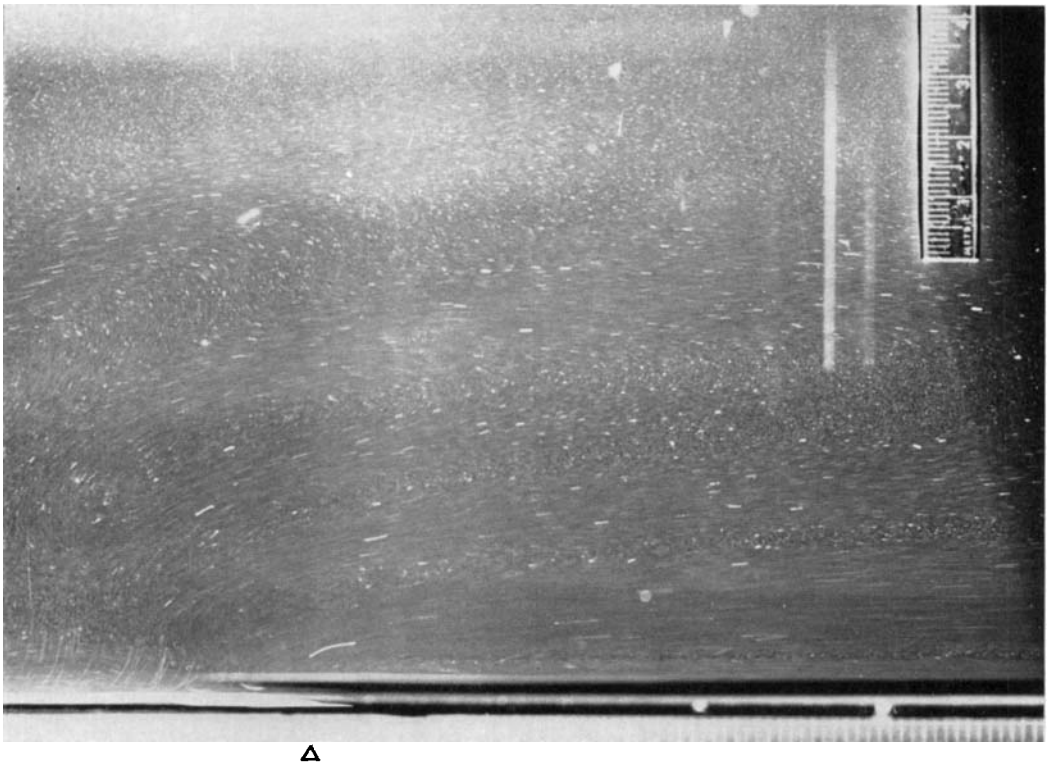

FIGURE 15. Flow field over the back of the plate 91·5 cm long for $F = 2{\cdot}84\ 10^{-2}$. Plate is moving from right to left past stationary camera. Arrow marks mean position of the back of the plate.

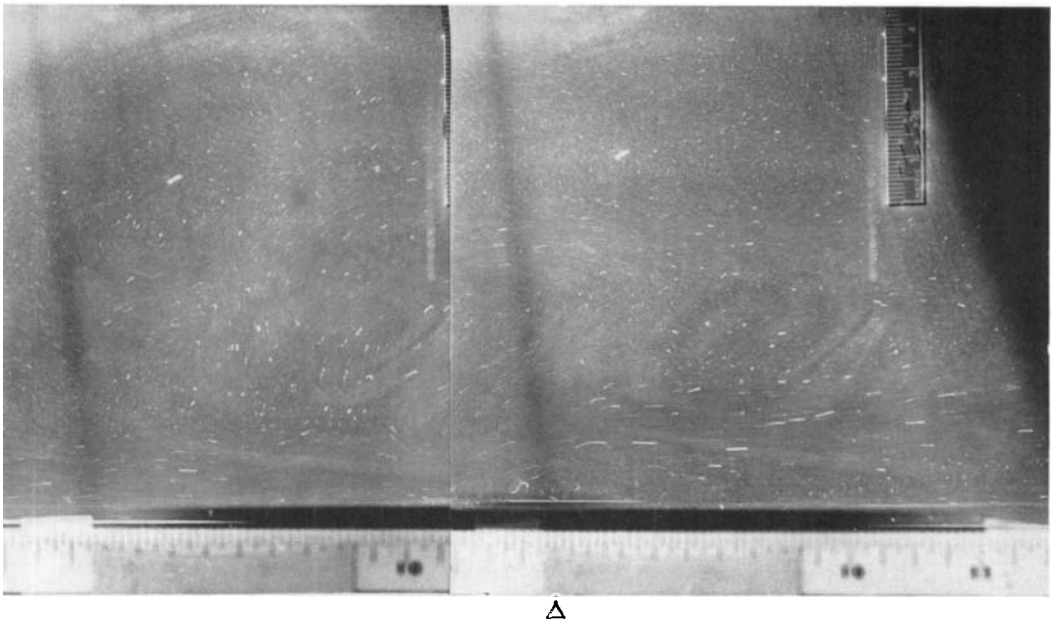

FIGURE 16. Velocity field of plate 0·635 cm long for $F = 2{\cdot}88 \times 10^{-2}$. Plate moves from left to right past the stationary camera. Arrow marks mean position of the centre of the plate.